ARTICLE NO. 79-1490R

Modeling of cw Chemical Laser with Annular Unstable Resonator

Tien Tsai Yang*
Rockwell International, Canoga Park, Calif.

An analytical model for predicting optical performance of a cw chemical laser has been developed. The model is constructed in which mixing, kinetics, and stimulated emission are coupled with a half-symmetric-unstable resonator with intercavity axicon (HSURIA). The formulation has been tested by anchoring to experimental small signal gain and closed-cavity power. The mixing parameters established from the data anchoring are used to examine the role of the resonator magnification, medium gain length, lasing line selection, optical axis location, and mode width in predicting laser performance. The dependence of laser performance trends on resonator parameters is predicted by the numerical results of the present study. Other resonator parameters affecting the power extraction have also been identified.

Nomenclature

A = reaction zone area, cm^2
a = feedback mirror radius, cm
B = Einstein coefficient
C_p = specific heat
D = $2Ma$, output beam diameter, cm
f = focal length of lens, cm
g = gain coefficient, cm^{-1}
h = enthalpy, erg/s; or Planck constant
H = defined by Eq. (4a)
I = radiation intensity, W/cm^2
$\bar{I}$ = average radiation intensity, W/cm^2
J = rotational quantum number
K = Boltzmann constant
L = empirical mixing length, cm
L_G = medium gain length, cm
l = distance between the centerlines of the fuel and oxidizer nozzles
M = Mach number; or resonator magnification
m = axicon magnification
$\dot{m}$ = mass flowrate, g/cm
N_0 = Avogadro's number
P = pressure, Torr
$P_v(J)$ = P branch transition line
Q = energy removal due to radiation effect, erg
r = radial coordinate; or optical ray height, cm
r' = optical ray slope
r_N = nozzle exit radius, cm
r_c = optical axis location, cm
r_g = $r_c - r_N$ = optical gap, cm
T = temperature, K
V = velocity, cm/s
v = vibrational quantum number
W = molecular weight, g/mole; or optical mode width, cm
γ = ratio of specific heat
ρ = density, g/cm^3
β = optical ray angle
β_c = mole of He in combustor/mole of F_2 available for lasing
β_N = mole of He in fuel nozzle/mole of F_2 available for lasing
[ ] = mole concentration, mole/g

Subscripts

a = annular region
c = compact region
f = fuel
o = oxidizer
s = species

Superscripts

0 = reference quantity

Received June 15, 1979; presented as Paper 79-1490 at the AIAA 12th Fluid and Plasma Dynamics Conference, Williamsburg, Va., July 24-26, 1979; revision received Jan. 8, 1980.

Index categories: Lasers; Reactive Flows.

*Member of Technical Staff, Rocketdyne Division. Member AIAA.

I. Introduction

INTERACTION between a confocal unstable resonator with cw diffusion chemical lasers has been investigated by means of geometric optics by Mirels[1] and physical optics by Sentman.[2] Both of these studies employed a linear gain volume as opposed to annular laser. These models vary significantly in their ability to model optical performance of cw chemical lasers in a manner that approximates the actual physical mechanism. Both Mirels and Sentman adopted a simplified single line kinetics approximation. In addition, the flow velocity and pressure of lasing gas are assumed constant in their model. Recently, a half-symmetric-unstable resonator with intercavity axicon (HSURIA) was proposed by Mumola et al.[3] for extracting power from a high-power, annular-gain volume laser. However, the experimental study of this HSURIA resonator, to date, has been concerned with laser output beam quality and its sensitivity to resonator misalignments for a flash photoysis DF laser and a cw electrical discharge He-Xe laser rather than a cw diffusion chemical laser. It is the purpose of this paper to investigate analytically the coupling between a HSURIA resonator and a cw diffusion type chemical laser.

In a cw diffusion chemical laser, supersonic mixing, chemical reaction, deactivation, and multispectral lasing occur simultaneously. The DF/HF gain medium cannot be adequately described in terms of a fixed small signal gain or gain distribution or a fixed gain saturation parameter. Instead, an analytical highly interactive model must be developed with mixing-kinetics and radiation-induced emission coupled to the resonator geometry in order to predict extractable power for a given resonator configuration. To examine the role of the optical resonator magnification, mode width, optical axis location, gain length, and lasing line selection in predicting cw chemical laser performance, an

elaborate fluid dynamic mixing model would complicate the analysis. In this analysis, the complex kinetics and fluid dynamic radiative interactions that occur in the laser cavity are computed by a simplified model in which the lasing species is treated as a multilevel molecule in rotational equilibrium; the fluid mixing model makes use of scheduled mixing; and the gain medium is approximated by a gain sheet. With these approximations, the qualitative behavior of the laser performance can be investigated.

In Sec. II, the coupled mixing, kinetics equations, and optical resonator and radiation field-medium interaction models that formulate the analytical model are given. In Sec. III, the analytical model is tested by anchoring to experimental small signal gain and closed-cavity power. In Sec. IV, the output power from a chemical laser with an annular (HSURIA) resonator is estimated. Finally, discussion and conclusion are summarized in Sec. V.

II. Formulation

A cw diffusion chemical laser that employs a HSURIA resonator is shown in Fig. 1. Annular cylindrical gain generator contains multiple fuel and oxidizer nozzle pairs, which are used to expand and mix fuel and oxidizer flow. The reaction between D_2 and F creates vibrational excited DF that lases and expands radially in the laser cavity. The optical axis is at $r=r_g$ downstream of the nozzle exit plane. The present coordinate systems are also shown in Fig. 1. In the following sections, a simplified model of laser medium is discussed, geometric model of the optical resonator is described, and a radiation field-lasing medium interaction model is given.

Simplified Model of Lasing Medium

The flow model configuration under consideration is depicted in Fig. 2. The flowfield is divided into three fundamental regions, consisting of the fuel and oxidizer streams and a mixing region. The flowfield in the mixing zone is assumed to be uniformly mixed. The fuel and oxidizer streams are further divided into a number of streamtubes. The analysis uses a quasi-one-dimensional flow model with mixing at specified scheduled rates between the multiple fuel and oxidizer streamtubes. Chemical reactions are allowed to occur within the mixing region. One-dimensional analysis is assumed to be applicable for both reaction region streamtube and each of the streamtubes in the fuel and oxidizer region. The conservation equations of mass, momentum, energy, and species for one-dimensional flow are discussed in detail in Ref. 4. These equations may be conveniently written as (for notation see Nomenclature):

$$\frac{dP}{P}=\frac{d\rho}{\rho}+\frac{dT}{T}-\frac{dW}{W} \tag{1}$$

$$\frac{d\rho}{\rho}=\frac{d\dot{m}}{\dot{m}}-\frac{dV}{V}-\frac{dA}{A} \tag{2}$$

$$\frac{dV}{V}=-\left[\frac{d\dot{m}}{\dot{m}}-\frac{V_o}{V}\frac{d\dot{m}_o}{\dot{m}}-\frac{V_f}{V}\frac{d\dot{m}_f}{\dot{m}}\right]-\frac{1}{\gamma M^2}\frac{dP}{P} \tag{3}$$

$$\frac{dT}{T}=-(\gamma-1)M^2\frac{dV}{V}-\frac{dQ+dH}{C_pT} \tag{4}$$

where

$$dH\equiv\sum_s h_s dY_s+\left[h+h_o+\frac{V^2-V_o^2}{2}\right]\frac{d\dot{m}_o}{\dot{m}}+\left[h-h_f+\frac{V^2-V_f^2}{2}\right]\frac{d\dot{m}_f}{\dot{m}}$$

$$d\dot{m}=d\dot{m}_o+d\dot{m}_f \quad h=\sum_s Y_s\left(\int_{T^0}^{T}C_{ps}dT+h_s^0\right) \tag{4a}$$

where subscripts o and f denote for oxidizer and fuel, respectively, and Y_s is species mass fraction. In the energy equation, dQ is the heat removal from the stream due to the effects of radiation and dh is the sum of the enthalpy change due to chemical reaction and temperature change.

The above equations apply for the reaction region and each of the streamtubes in the fuel and oxidizer regions. An additional simplification has been applied to the latter regions. Specifically, it is assumed that the flowfield external to the mixing region is nonreacting and isentropic. Under these conditions, the equations given can be reduced to sums of total differentials. The final simplification applied to the equations given is the assumption that the transverse pressure gradients may be neglected. In Appendix A, a method for handling the external flow is discussed.

The effect of diffusion is accounted for by the empirical mixing rates that are used to simulate the complex process of mass diffusion to the mixing layer. The equations that have been used herein are based on the results of solutions to the diffusion equation. That is, it has been assumed that the amount of mass remaining in either the fuel or oxidizer may

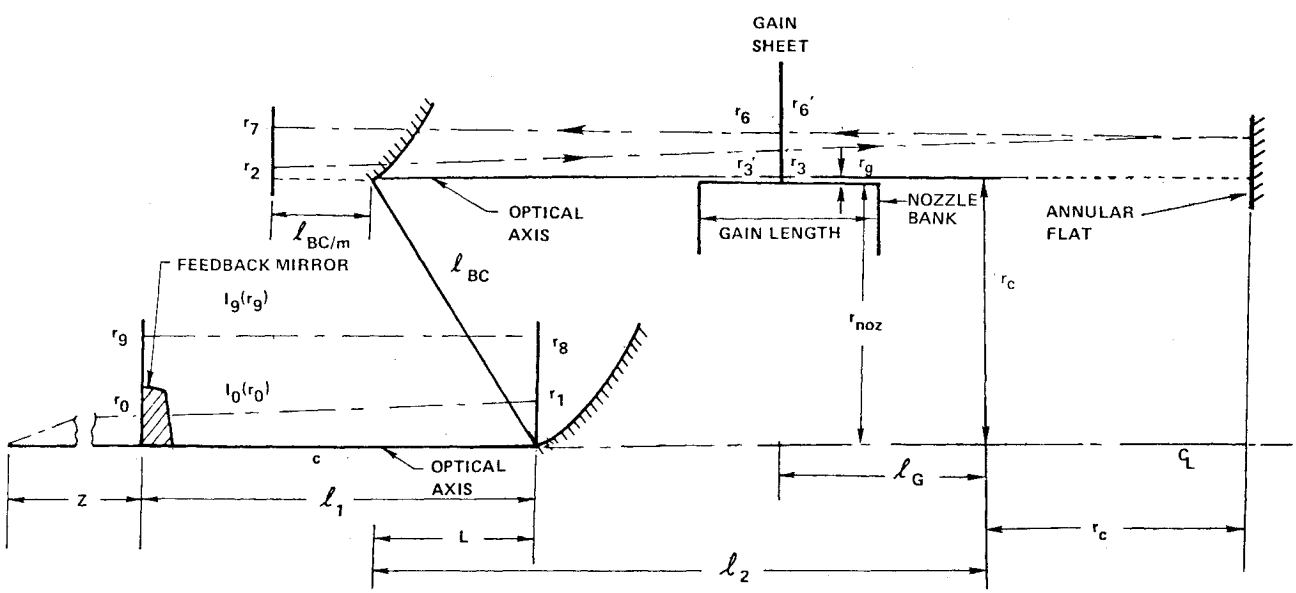

Fig. 1 Half-symmetric-unstable resonator with intercavity axicon.

be described by an error function

$$\dot{m}=\dot{m}_o\left\{1-\left[\mathrm{erf}^2\left(\frac{r-r_0}{L_m}\right)^{1/2}\right]\right\} \tag{5}$$

For turbulent flow mixing, a linear mixing function is used frequently

$$\dot{m}=\dot{m}_o\left\{1-\left(\frac{r-r_0}{L_m}\right)\right\} \tag{6}$$

where $\dot{m}$ is the amount of mass remaining in either the fuel or oxidizer streams at position r, $\dot{m}_o$ is the initial mass flow when $r=r_0$ and L_m is the mixing length. As a result of the above formulation, the mixing mechanism in the cavity is modeled by two empirical parameters (L_{mo} and L_{mf}). Flow velocity and temperature profiles for both the fuel and oxidizer at the cavity entrance location are those Launder-type solutions for the boundary layers.[5] The mass flow required by the reaction zone is provided by the sets of the streamtubes that model the discrete flow properties (initial profiles) of the fuel and oxidizer streams. Each streamtube is initialized with certain mass flux $\dot{m}$ and is fully depleted before Eqs. (5) and (6) are allowed to access the next streamtube in the sequence.

The reaction between D_2 and F creates vibrational excited DF that is subsequently deactivated by collisions and by radiation. The following reactions are considered in the present study.

Chemical Pumping

$$\begin{gathered}\mathrm{F}+\mathrm{D}_2(0)\rightleftharpoons\mathrm{DF}(v)+\mathrm{D}\\ \mathrm{F}+\mathrm{D}_2(v')\rightleftharpoons\mathrm{DF}(v)=\mathrm{D}\quad(v'>0)\\ \mathrm{D}+\mathrm{F}_2\rightleftharpoons\mathrm{DF}(v)+\mathrm{F}\end{gathered} \tag{7}$$

Vibrational-Translation ($v-T$) Deactivation

$$\begin{gathered}\mathrm{DF}(v)+\mathrm{DF}\rightleftharpoons\mathrm{DF}(v-1)+\mathrm{DF}\\ \mathrm{DF}(v)+\mathrm{F}_2\rightleftharpoons\mathrm{DF}(v-1)+\mathrm{F}_2\\ \mathrm{DF}(v)+\mathrm{He}\rightleftharpoons\mathrm{DF}(v-1)+\mathrm{He}\\ \mathrm{DF}(v)+\mathrm{D}\rightleftharpoons\mathrm{DF}(v')+\mathrm{D}\\ \mathrm{DF}(v)+\mathrm{F}\rightleftharpoons\mathrm{DF}(v')+\mathrm{F}\\ \mathrm{DF}(v)+\mathrm{HF}\rightleftharpoons\mathrm{DF}(v-1)+\mathrm{HF}\\ \mathrm{DF}(v)+\mathrm{D}_2\rightleftharpoons\mathrm{DF}(v-1)+\mathrm{D}_2\\ \mathrm{D}_2(v)+\mathrm{M}\rightleftharpoons\mathrm{D}_2(v-1)+\mathrm{M}\end{gathered} \tag{8}$$

Vibrational-Vibrational ($v-v$) Quantum Exchange

$$\begin{gathered}\mathrm{DF}(v)+\mathrm{DF}(v')\rightleftharpoons\mathrm{DF}(v+1)+\mathrm{DF}(v'-1)\\ \mathrm{DF}(v)+\mathrm{D}_2(v')\rightleftharpoons\mathrm{DF}(v+1)+\mathrm{D}_2(v'-1)\\ \mathrm{DF}(v)+\mathrm{N}_2(0)\rightleftharpoons\mathrm{DF}(v-1)+\mathrm{N}_2(1)\end{gathered} \tag{9}$$

Excited DF is created by the pumping reaction [Eq. (7)]. Deactivation by single quantum jump is governed by the vibrational-translation reaction [Eq. (8)], and vibrational-vibrational reaction [Eq. (9)].

In the $V-T$ deactivation, multiquanta transitions resulting from interactions with D and F atoms are included based on the theoretical finding of Wilkins.[6] The rate constants used in the present study are those reported in Ref. 7, except that the $V-T$ deactivations of DF by D and HF are increased by 30 times and 3 times, respectively. These were the best estimates at the time of this study. Inasmuch as research on the chemical kinetics of the D_2-F_2 system is still in progress, one might expect further changes in rate coefficients. Since the rotational relaxation process apparently is fast enough at pressure of practical interest to maintain Boltzmann rotational distribution, it is assumed that the DF molecules in each vibrational level are in rotational equilibrium at the local translational temperature.[8] Finally, the line center P-branch radiative transition is assumed.

The local gain coefficient is derived based on the DF population difference between two rotational-vibrational states. If J is the rotational quantum number of the rotational state corresponding to vibrational state $V-1$, and $J-1$ is the rotational quantum number of rotational state corresponding to vibrational state V, then the local gain coefficient for a transition from a state $(V, J-1)$ to state $(V-1, J)$, $g^{V,J-1}_{V-1,J}$ is,

$$g^{V,J-1}_{V-1,J}=h\omega^{V,J-1}_{V-1,J}S(\omega^{V,J-1}_{V-1,J})\rho N_0\{[\mathrm{DF}(v,J-1)]B^{V,J-1}_{V-1,J}-[\mathrm{DF}(V-1,J)]B^{V-1,J}_{V,J-1}\} \tag{10}$$

where $B^{V,J-1}_{V-1,J}$ is the Einstein coefficient for the induced transition, $\omega^{V,J-1}_{V-1,J}$ is the resonant frequency, S is the normalized shape factor at the resonance frequency, and N_0 is Avogadro's constant.

The differential equation for the distribution of DF(V) along flow-direction can be expressed by

$$\frac{\mathrm{d}[\mathrm{DF}(V)]}{\mathrm{d}r}=\left\{\frac{\mathrm{d}[\mathrm{DF}(V)]}{\mathrm{d}r}\bigg|_{\mathrm{chem}}+\frac{\mathrm{d}[\mathrm{DF}(V)]}{\mathrm{d}r}\bigg|_{\mathrm{relax}}+\frac{\mathrm{d}[\mathrm{DF}(V)]}{\mathrm{d}r}\bigg|_{\mathrm{rad}}\right\}-\frac{1}{\dot{m}}[\mathrm{DF}(V)]\left\{\frac{\mathrm{d}\dot{m}_o}{\mathrm{d}r}+\frac{\mathrm{d}\dot{m}_f}{\mathrm{d}r}\right\} \tag{11}$$

The first term on the right-hand side of Eq. (11) represents the creation of DF(V) by the chemical pumping reaction while the second and third terms represent deactivation by collision and by radiation stimulated emission, respectively. The last term on the right-hand side of Eq. (11) represents the mixing contribution from oxidizer and fuel streams to reaction zone. The terms $\mathrm{d}\dot{m}_o/\mathrm{d}r$ and $\mathrm{d}\dot{m}_f/\mathrm{d}r$ in Eq. (11) are specified by the gas dynamics mixing analysis [Eqs. (5) and (6)]. The calculation for the chemical production and collisional deactivation can be obtained based on the chemical reactions given in Eqs. (7-9). The radiation induced production term

$$\frac{\mathrm{d}[\mathrm{DF}]}{\mathrm{d}r}\bigg|_{\mathrm{rad}}$$

in Eq. (11) can be written as

$$\rho u\frac{\mathrm{d}[\mathrm{DF}(V)]}{\mathrm{d}r}\bigg|_{\mathrm{rad}}=\sum_J\left[\frac{\tilde{I}^{V+1,J-1}_{V,J}g^{V+1,J-1}_{V,J}}{hc\omega^{V+1,J-1}_{V,J}N_0}-\frac{\tilde{I}^{V,J}_{V-1,J+1}g^{V,J}_{V-1,J+1}}{hc\omega^{V,J}_{V-1,J+1}N_0}\right] \tag{12}$$

where $\tilde{I}^{V,J-1}_{V-1,J}$ is the radiation intensity at the resonant frequency $\omega^{V,J-1}_{V-1,J}$ and h is Planck constant. The summation over J is required to account for multiline lasing between an upper and lower vibrational state. Equation (12) accounts for radiation-medium interaction process, and the value of $\tilde{I}$ will be discussed in detail in a later section.

Geometric Optics Model

An experimental study of several unstable resonator concepts for annular cylindrical mode volume laser has been performed by Mumola et al.[3] Such concepts are relevant to

the development of more compact lasers with high specific energy and more uniform volumetric excitation. The annular geometry is potentially advantageous for cw lasers employing radial flow (outward) of gain media. The annular configuration allows for large volume excitation even when the transverse extent of the gain region (annular width) is limited. Practical exploitation of this geometry requires new laser resonator concepts of which several have been discussed recently by Chodzko et al.,[9] Casperson,[10] and Frieberg et al.[11]

The resonator system to be modeled in this analysis is a half symmetric unstable resonator with intercavity axicon (HSURIA), see Fig. 1. Furthermore, the axicon (beam compactor) shown uses confocal parabolas of revolution, that is, they are toric elements with a common ring focus. The detailed derivation of this resonator is given in Appendix B.

Using the results discussed in Appendix B, the ray heights, the round trip intensity distribution, and the feedback power of the resonator system are obtained as follows (see Fig. 1):

1) Edge ray heights at annular flat and gain sheet:

$$(r_4 - r_c)_{\max} = W = \frac{M+1}{2} \cdot \frac{a}{m}; \quad a = \frac{D}{2M} \tag{13}$$

$$(r_6 - r_c)_{\max} = Wg = \frac{M+1}{2} \cdot \frac{a}{m} + m\left[\frac{a(M-1)}{2l_{eq}}\right](l_G + r_c) \tag{14}$$

2) Round trip intensity:

$$I_{FB}(r_9) = I_0(Mr_0) = BG_3(r_3)G_6(r_6)I_0(r_0) \tag{15}$$

where

$$B \equiv (1-A_{FB})(1-A_R)^2(1-A_{BC})^2(1-A_{RC})^2/M^2$$

and $G_3(r_3)$ and $G_6(r_6)$ are the total gain coefficients and A_{FB}, A_R, A_{BC}, and A_{RC} are mirror absorption coefficients

3) Feedback power:

$$P_{FB} = 2\pi \int_0^a dr_0 r_0 I_0(r_0) = 2\pi \int_0^a dr_g r_g I_{FB}(r_g) \tag{16}$$

At stations 3 and 6 (see Fig. 1), radiation fields interact with gain medium. A discussion of this interaction is given in the subsequent section.

It should be noted that once the magnification M, optical axis r_c, and lasing zone width W are defined, the optical analysis for an annular gain medium with HSURIA resonator is identical to that for a linear gain medium with conventional cylindrical unstable resonator. This is demonstrated in Appendix B.

In theory, geometric-optics analysis is accurate only at large Fresnal number N. However, diffraction calculations by Rensch and Chester[12] on rectangular-mirror confocal resonator show that for $N>5$ the geometric optics approximation gives a fairly good estimate of beam steering effects. Since the primary interest in present analysis is emphasized on radiation field/flowfield interaction, and the interaction scheme for geometric optics is believed to be the same as that of wave optics, therefore, geometric optics approximation should provide a fairly good estimate of gross laser performance.

Simplified Model of Radiation Field-Lasing Medium Interaction

The detailed analysis of the radiation field-lasing medium is extremely complicated. In a high-power laser, the active medium saturates and therefore the medium becomes nonlinear. In a nonlinear active medium, the power gain coefficient is not only a function of spatial position but also a function of the spatial radiative flux intensity. To simplify the analysis of an active cavity, the idea of concentrating the lasing medium into infinitely thin sheets is assumed.[13] With this assumption, the optical ray propagation in the cavity takes place in the free space outside the sheet, the loaded gain becomes independent of z (optical ray direction), and the calculations are simplified.

The radiation-medium interaction occurs as a result of the net two-way intensity $\tilde{I}(z)$,

$$\tilde{I}(z) = I^+(z) + I^-(z) \tag{17}$$

where $I^+(z)$ and $I^-(z)$ are the intensity in the positive and negative directions, respectively.

To be consistent with the gain sheet approximation, which involves attributing the medium properties to a region of infinitely thin thickness in the propagation direction and coincident with the location at the center of gain length, it is appropriate to determine the average net two-way intensity in the gain region, $\tilde{I}$ as

$$\tilde{I} = \frac{1}{L_G}\int_{-L_G/2}^{L_G/2} [I^+(z) + I^-(z)]dz = \frac{(I_6 - I_6') + (I_3 - I_3')}{\bar{g}L_G} \tag{18}$$

where $\bar{g}$ is the average gain coefficient over a half-nozzle pair, L_G the total gain length, I_3' and I_6' the flux density going to the gain sheet, and I_6 and I_3 the flux density coming out from the gain sheet (see Fig. 1). In terms of local gain function G and local gain sheet coordinates x and x is measured from the nozzle exit cylinder, we have

$$\tilde{I}(x)\bar{g}(x)L_G = [G(r_6) - 1]I_6'(r_6) + [G(r_3) - 1]I_3'(r_3) \tag{19}$$

In general, we have

$$G = e^{\bar{g}L_G} \tag{20}$$

In the evaluation of Eq. (18), the radiative transfer equation

$$\frac{dI}{dx} = \bar{g}I \tag{21}$$

has been used.

The nature of the medium saturation is revealed by noting that the $\tilde{I}$ determined by Eq. (18) appears in Eq. (12). Note also that the $\bar{g}$ which appears in Eq. (18) is determined from Eq. (10).

For an unstable resonator, the gain sheet approximation should be valid provided that the optical beam does not geometrically expand appreciably throughout the active medium. Rensch and Chester[12] have done a study of the gain sheet approximation by comparing mode calculations that utilize a distributed multiple gain sheet ($\sim$20 sheets) model. From numerical calculations they found that the single gain sheet approximation broke down when $M \geq 3$. In Sec. IV, a comparison between the results obtained by a single gain sheet and five gain sheets will be given.

A geometric optics loaded cavity computer code (GOPWR) has been developed that employed the above described fluid dynamics, chemical kinetics, optical resonator, and radiation interaction model. With the GOPWR code, we will establish the mixing model parameters by anchoring experimental small signal gain and closed cavity power, and then investigate the effects of resonator magnification, medium gain length lasing line selection, and mode width on cw DF laser optical performance.

III. Analysis: Experimental Data Anchoring

The validity of the present analytical formulation and mixing model selection can be best tested by reproducing experimental data. The small signal gain, shroud wall pressure, and closed cavity power measured by Bell Aerospace were anchored. The results are discussed below.

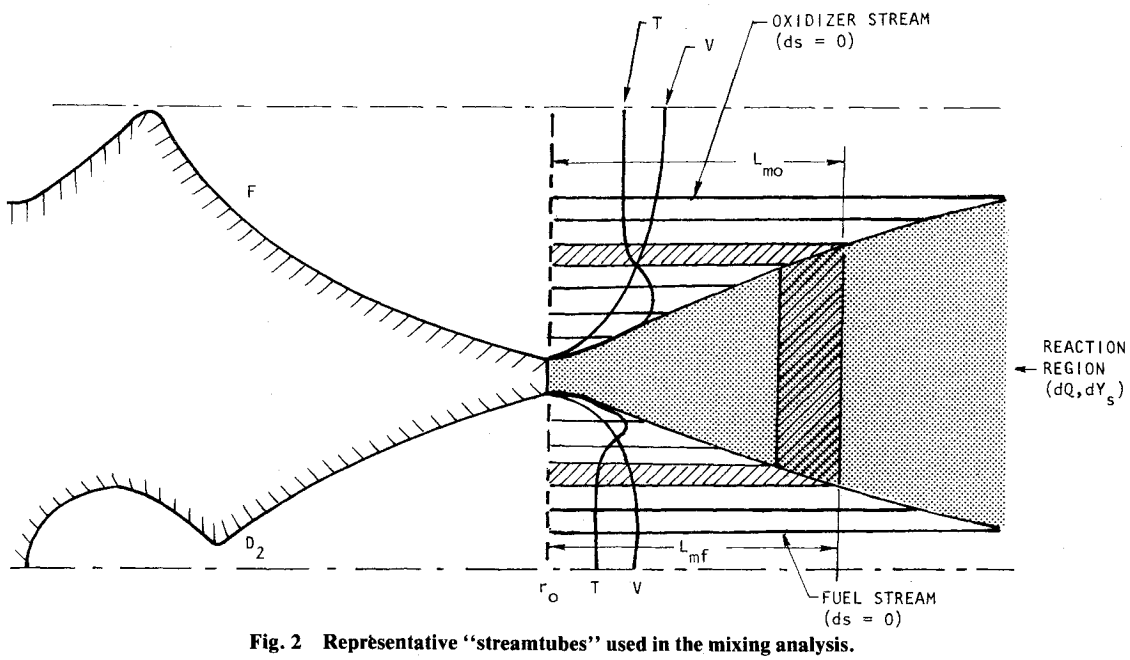

Fig. 2 Representative "streamtubes" used in the mixing analysis.

Small Signal Gain Anchoring and Mixing Length Selection

One of the important parameters in determining the fluid flow mixing is the diffusion model. This has always been a difficult problem in the analysis of chemical reacting flow. The present analysis makes use of scheduled mixing functions. With this mixing model, the mixing mechanism occurring in the cavity is modeled by two empirical parameters. One is used to specify the fuel stream mixing, the other for the oxidizer stream.

It can be assumed that the correct choice for mixing lengths are those that give results in agreement with experiment. The experimental small signal gain data used for establishing the mixing length were obtained from a Bell Aerospace HF Technology Program with C1-XI nozzle. The DF lasing small signal gain data for the combustor and nozzle diluent ratio of $\beta_C/\beta_N = 15/40$ is shown in Fig. 3.[14] A more complete description of the terminology for combustion driven chemical laser is given by Wilson and Hook.[15] Using Bell test conditions as the input to the combustor and nozzle code (CSONCA), the velocity, temperature and concentration profiles, and pressures for fuel and oxidizer streams at nozzle exit plane were calculated. The effect of nozzle wall recombination is accounted for by assuming that the F atom concentration profile is a one-third recombination profile computed from LAMP code. One-third recombination profile is a profile similar in shape with the fully catalytic wall concentration profile obtained from the LAMP code, except, instead of zero concentration of F atom at wall, the wall concentration was set equal to one-third of the frozen concentration. With these flow properties, the GOPWR code was used to calculate the small signal distributions. The calculated small signal gains are plotted in Fig. 3 along with Bell's data for comparison. In general, close agreement between the calculation and experiments can be seen in Fig. 3. $P_1(J)$ lines do not agree well with the experimental data; this is most likely due to too large a deactivation rate of $V=1 \rightarrow V=0$. The small signal gain curves of Fig. 3 were obtained by using a linear mixing function [Eq. (6)] with mixing lengths 7.5 and 9 cm for oxidizer and fuel streams, respectively.

Bell's experiment was conducted with a linear cavity. Our flow model has been developed for radial flow. It was assumed that the linear cavity flow can be simulated by an equivalent radial flow. Since flow expansion within the lasing cavity is not precisely known and may, in fact, vary with position, the selection of nozzle radius r_N for simulating linear flow is difficult to justify. In the present analysis, the effective flow expansion, which is assumed to be the cavity geometric area with boundary layer displacement thickness correction, is represented by a radial expansion flow with a single radius r_N. Therefore, the flow was assumed under a uniform expansion with expansion ratio defined as $(\Delta r_N + r_N)/r_N$, where Δr is lasing zone length. Thus for a fixed Δr, the smaller the r_N, the larger the effective flow expansion.

Cavity Wall Pressure Anchoring

Cavity wall pressure distributions were also measured by Bell Aerospace for the same flow conditions.[16] Because of the nature of a large transverse pressure gradient in supersonic reacting flow, wall pressure may not necessarily represent the actual pressure in the reaction zone. Furthermore, if the argument of zone of silence, which is hard to define for a highly nonuniform flow such as most of the cavity flow, is valid, cavity pressure may not have real physical connection with the reaction zone. In spite of these facts, cavity wall pressure has been believed to be a useful indicator for chemical reaction processes. The pressure anchoring was taken as a step to justify the selection of effective cavity expansion.

Figure 4 shows the experimental wall pressure distributions for $\beta_C/\beta_N = 15/40$. The calculated pressure is also included in the same figure for comparison. The experimental wall pressure distribution trend was reasonably reproduced. The calculated values show higher in the initial region and lower in the downstream region than experimental data. This characteristic is to be expected since the real nonuniform cavity expansion was calculated by using a uniform expansion configuration resulting from using a single radius.

Closed Cavity Power Anchoring

Having selected the mixing function and length from small signal gain anchoring, one may now proceed with closed cavity power calculation. Figure 5 shows the normalized measured specific power vs $2X_c$ (lasing zone).[16] Since closed cavity is a measurement of potential laser output power, it is important to check that the analytical results reproduce the experimental results. At the same time, this exercise provides another check of the mixing length obtained from small signal gain anchoring. It is believed that one can approximately estimate the closed cavity power for cw DF/HF chemical

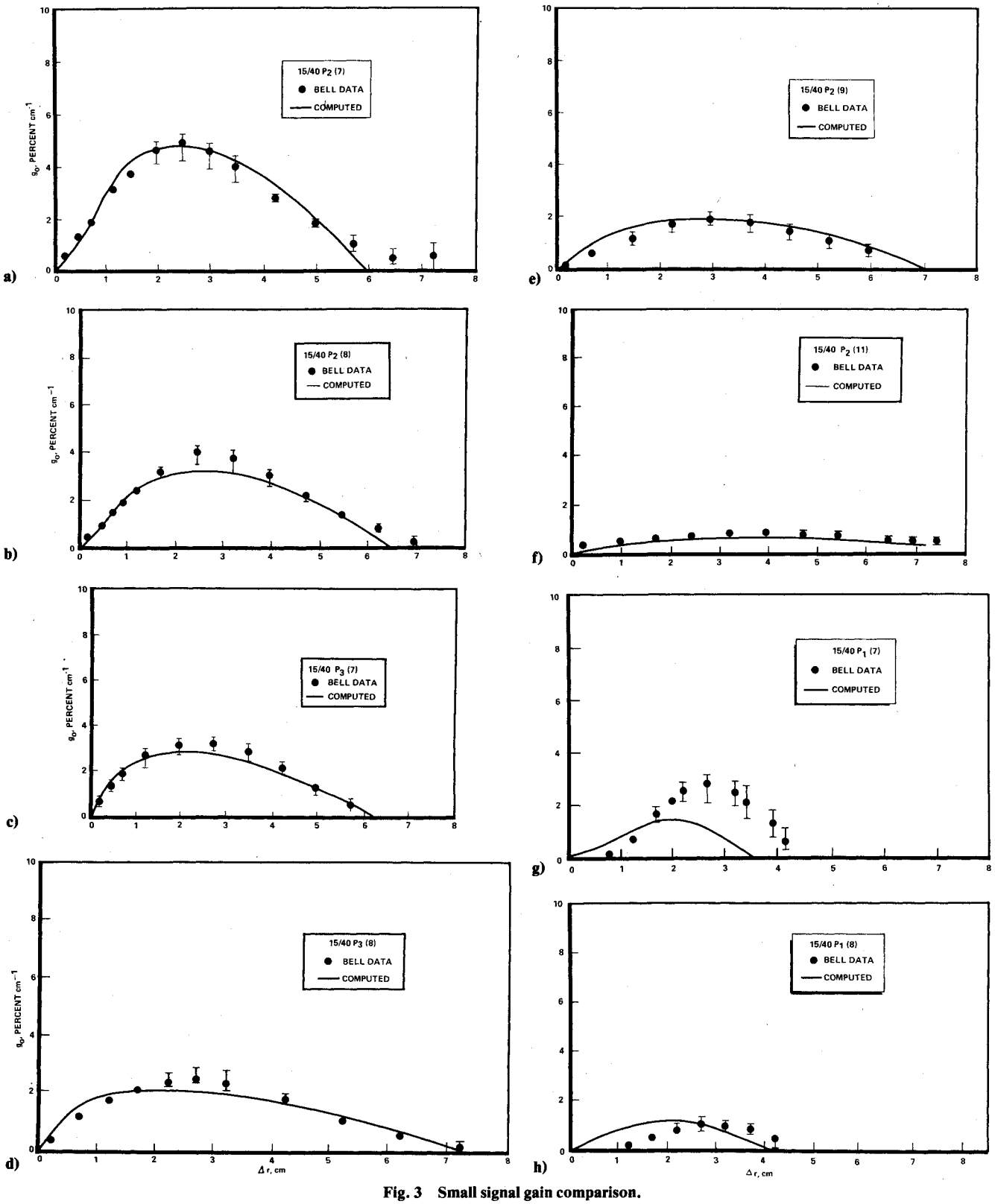

Fig. 3 Small signal gain comparison.

lasing by letting the resonator magnification approach one ($M \rightarrow 1$) in the GOPWR calculation, but this has not yet been proven mathematically. With this assumption, closed cavity power was calculated. The results obtained with $P_1(11)$, $P_2(11)$, and $P_3(11)$ are plotted in Fig. 5 for comparison. It can be seen that the measured specific power is reasonably reproduced. The good agreement obtained was for a fixed cavity configuration and a set of mixing lengths; however, these results do not necessarily imply that these values of mixing length and cavity are the correct or unique choice necessary to understand the real physical phenomena. An important point here is that a single set of mixing lengths can simultaneously reproduce the experimental small signal gain, shroud wall pressure, and closed cavity power.

Closed cavity power is expected to result from different P branches of the same vibrational band. The prediction shown in Fig. 5 was calculated using lines selected to give the maximum power. In this analysis, the lasing lines of $P_v(11)$, with $v = 1, 2$, and 3 were used. It was found that the maximum line closed cavity power approximately agrees with the ex-

perimental multiline closed cavity power. However, the ability to anchor closed cavity power is still not as complete as desired since the detailed spectral content cannot yet be predicted. This is a shortcoming of the basic model rather than a difficulty of anchoring.

Additionally, the resonator employed is different from those used in the closed cavity power measurement. Because the medium is almost completely saturated when $M \to 1$, the details of the resonator configuration becomes unimportant.

IV. Outcoupled Power Analysis

Once the mixing length has been selected, the effects of the laser medium and resonator parameter on cw DF chemical laser optical performance can be investigated. These parameters include combustion-nozzle diluent ratio (β_C/β_N), resonator magnification (M), medium gain length (L_G) lasing line selection (J), mode width (W), and optical axis location (r_c).

The variation of near-field output power with resonator magnification M is shown in Fig. 6 for the flow condition of $\beta_C/\beta_N = 15/40$. The results were calculated for a mode width $W = 5$ cm, and for lasing line $P_v(8)$, $P_v(9)$, $P_v(10)$, and $P_v(11)$ with $v = 1$, 2, and 3, and for an optical gap (the distance between optical axis and nozzle exit plane) $r_g = 0.8$ cm.

The calculations shown in Fig. 6 can be best explained by the following simplified saturation model. In the geometric optics limit, the threshold gain of the resonator is approximately given by[17]

$$\frac{g_t}{g_0} = \frac{1}{2L_G g_0} \ln\left(\frac{M^2}{R_1 R_2}\right) \tag{22}$$

where R_1 and R_2 are mirror reflectivities, M is the cavity magnification, and L_G is the length of the gain medium. Thus, for a specific L_G, there is a cavity magnification M that yields a desirable gain g_t. It is desirable for the medium to be saturated, with g_t a small fraction of unsaturated gain g_0, since the relative efficiency of laser power extraction is approximately proportional to $(1 - g_t/g_0)$. It is seen from Eq. (22) that the gain saturation and hence the output power of a laser device improves with increasing gain length L_G and decreasing magnification M. This is illustrated by the results given in Fig. 6. As magnification M reaches to ≈ 1.005, the outcoupled power shown in Fig. 6 begins to fall off. As we may expect, that the power falloff is due to a vanishingly small output coupling.

Also shown in Fig. 6 is the much stronger effect magnification has on outcoupled power for high rotational lines than for low rotational lines. Saturation in high J is, as expected, more difficult to achieve than in low J because of the lower small signal gain of high J. With decreasing magnification M, the radiation within the cavity becomes large enough to saturate higher J and hence increases output power.

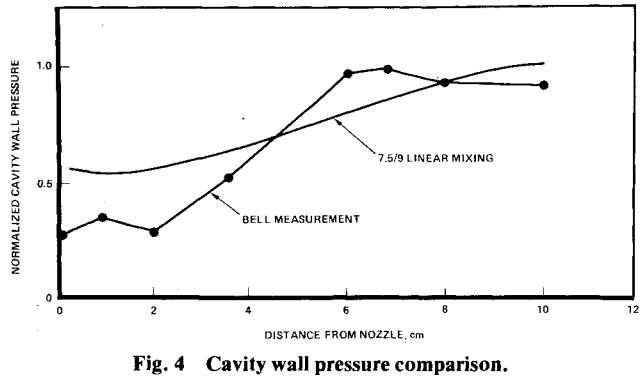

Fig. 4 Cavity wall pressure comparison.

Shown in Fig. 7 is that the output power increases with increasing gain length. These calculations were obtained for a magnification $M = 2$ with lasing lines $P_1(9)$, $P_2(9)$, and $P_3(9)$. The behavior of this result is again clearly implied by Eq. (22). Therefore, laser performance should be evaluated based on a combined effect of resonator magnification M and medium gain length L_G, i.e.,

$$\frac{g_t}{g_0} = \frac{1}{2g_0 L_G} \ln\left(\frac{M^2}{R_1 R_2}\right)$$

rather than by M or L_G only.

The variation of output power with mode width W is shown in Fig. 8. These results were obtained for a magnification $M = 2$, for lasing lines $P_1(9)$, $P_2(9)$, and $P_3(9)$ and for $r_g = 0.8$ cm. For small mode width, only a small portion of gain volume was coupled with radiation field and hence output power is also small. Output power increased with increasing mode width

$$W_N = W/W = 5 \text{ cm}$$

and remains relatively constant for W_N between $0.7 \sim 1.1$, and begins to fall off at $W_N = 1.2$. The power falloff at large W_N is mainly due to negative gain absorption radiation coupling.

The effect of the optical gap r_g on output power is indicated in Fig. 9. The peak value of the output power, and the radial location of the peak moves downstream as the rotational quantum number J is shifted from $J = 7$ to 9. In general, near the nozzle exit plane, the small signal gain is higher for low values of J and hence the loaded gain is generally above the threshold gain. With increasing r_g, the gain for high J values becomes larger and the output power increases. Since the gain cutoff distance decreases with decreasing J, the output power falls off faster as J is shifted from high to low values.

To assess the validity of the present geometric optics model, it is necessary that some comparison be made with a physical optics model. Shown in the dotted line in Fig. 6 is the result obtained by a physical optics model calculated with $P_1(8)$,

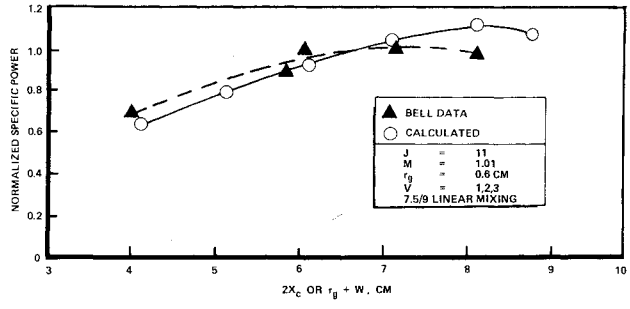

Fig. 5 Closed-cavity power comparison.

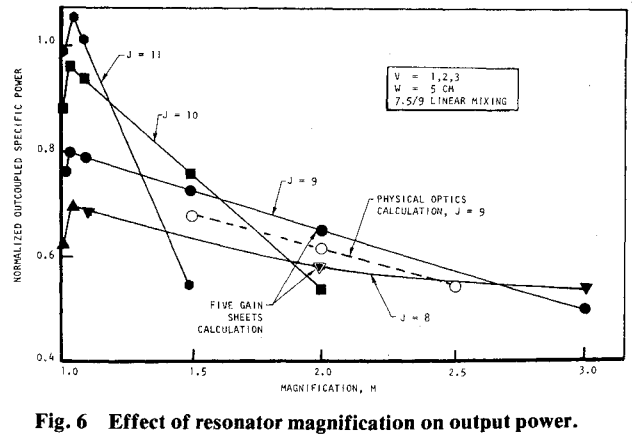

Fig. 6 Effect of resonator magnification on output power.

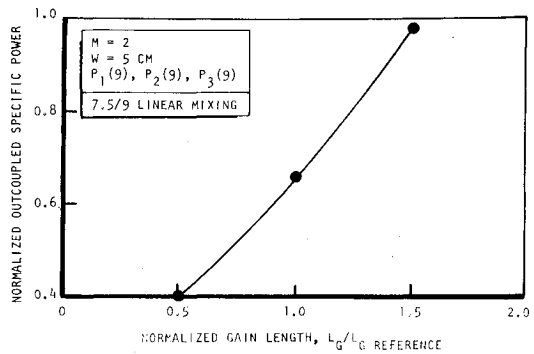

Fig. 7 Effect of medium gain length on output power.

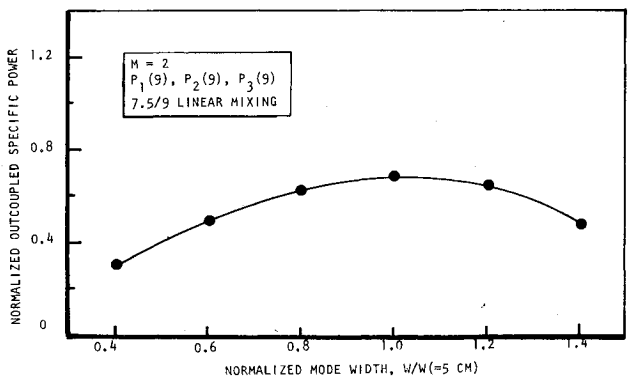

Fig. 8 Effect of resonator mode width on output power.

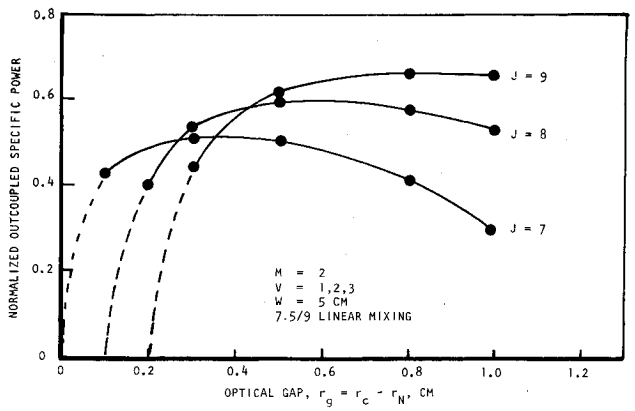

Fig. 9 Effect of resonator optical axis location on output power.

$P_2(8)$, and $P_3(8)$ for magnification $M=1.5$, 2, and 2.5. It is seen from Fig. 6 that the geometric optics predictions are in good agreement with those of physical optics within 10%. The lower prediction by physical optics model is mainly due to diffraction loss which is not included in geometric optics model.

Calculations were also made by a model with five gain sheets and the results are essentially the same as those obtained by a single gain sheet as indicated in Fig. 6.

V. Summary

A simplified model for predicting the laser performance for a chemical laser with an annular unstable resonator (HSURIA) has been presented. This model permits examination of the effects of resonator magnification, medium gain length, rotational lasing line, optical mode width, and optical axis location on power extraction efficiency. The output power predicted by this model is found to compare well (within 10%) with that by a more comprehensive model (physical optics). Therefore, we expect this model to be the logical tool for use in parametric studies. Once the range of parameters is defined, one can return to the more detailed calculations by physical optical model.

It may be concluded that the geometric optics model is useful in that it identifies the important physical parameters affecting power extraction and gain saturation. It does not, however, give information on the phase distribution of the output power or the beam quality. Because of the simplifications associated with the mixing and no diffraction loss, the power levels predicted by this model will be approximate. The model will be most useful as an indicator of trends.

Appendix A

In the present flow model, it is necessary to differentiate between the properties of the reaction region and those in the isentropic streamtubes. Variables pertaining to the streamtubes are subscript.

In a general flow configuration, the total cross-section area available to the flowfield is

$$A_T = A(r) + \sum_i A_i(r) \tag{A1}$$

where A is reaction zone area and A_i is isentropic streamtube area. Therefore

$$\frac{dA}{A} = \frac{dA_T}{A} - \sum_i \frac{dA_i}{A} \tag{A2}$$

Using isentropic relations and the assumption of no transverse pressure gradient, one obtains,

$$\frac{dA_i}{A_i} = \frac{d\dot{m}_i}{\dot{m}_i} - \frac{1}{\gamma_i}\left\{1 - \frac{\gamma_{i-1}}{2\left[\left(\frac{P_{oi}}{P}\right)^{\frac{\gamma_{i-1}}{\gamma_i}} - 1\right]}\right\}\frac{dP}{P} \tag{A3}$$

Using Eq. (A3) in Eq. (A2) and substituting the resulting equation into Eq. (1), dP/P can be expressed as

$$\frac{dP}{P} = \left\{[2+(\gamma-1)M^2]\frac{d\dot{m}}{\dot{m}} - \left[\frac{dA_T}{A} - \sum_i \frac{A_i}{A}\frac{d\dot{m}_i}{\dot{m}_i}\right] - [1+(\gamma-1)M^2]\cdot\left[\frac{V_o}{V}\frac{d\dot{m}_o}{\dot{m}} + \frac{V_f}{V}\frac{d\dot{m}_f}{\dot{m}}\right] - \frac{dQ+dH}{C_PT} - \frac{dW}{W}\right\} \div \left\{1 - \sum_i \frac{A_i}{\gamma_i A}\left[\frac{\gamma_{i-1}}{2}\left(\left(\frac{P_{oi}}{P}\right)^{\frac{\gamma_{i-1}}{\gamma_i}} - 1\right)^{-1} - 1\right] - \frac{1+(\gamma-1)M^2}{\gamma M^2}\right\} \tag{A4}$$

Similarly, Eqs. (A2) and (A3) can be combined with Eqs. (2-4) to provide three ordinary differential equations for dV, dT, and $d\rho$. In this manner, the flowfield variation along the streamlines in the mixing zone and the isentropic streamtubes is solved in a coupled fashion.

Appendix B

From ray optics analysis of curved mirrors and thin lenses, one can deduce that the behavior of a ray upon repeated bouncing back and forth between these mirrors will be exactly the same as the behavior of a ray passing through an iterated sequence of lenses. The ray paths through the two structures are the same, except that the ray pattern is folded in the resonator and unfolded in the lens sequence. The focal lengths

of the lens are the same as the focal lengths of the mirrors. The lens spacing is the same as the mirror spacing.

Consider the net transformation of a ray in passing through one complete round trip inside the resonator or one full period of the iterated periodic lens waveguide. When a ray passes through such a series of optical elements, the total or overall ray transformation and r and r' (where r and r' are the ray height and ray slope, respectively) can be computed by successive application of the individual (A, B, C, D) matrices; that is, successive multiplication of the ray vector by the individual ray matrices. If this procedure is applied to the sequence of elements shown in Fig. B1, the resulting overall transformation matrix for round trip propagation is [18]

$$P=\begin{pmatrix}1 & \ell_1\\ 0 & 1\end{pmatrix}\begin{pmatrix}1 & 0\\ -\frac{1}{f_1} & 1\end{pmatrix}\begin{pmatrix}1 & \ell_{BC}\\ 0 & 1\end{pmatrix}\begin{pmatrix}1 & 0\\ -\frac{1}{f_2} & 1\end{pmatrix}$$

$$\times\begin{pmatrix}1 & \ell_2+r_c\\ 0 & 1\end{pmatrix}\begin{pmatrix}1 & \ell_2+r_c\\ 0 & 1\end{pmatrix}\begin{pmatrix}1 & 0\\ -\frac{1}{f_2} & 1\end{pmatrix}\begin{pmatrix}1 & \ell_{BC}\\ 0 & 1\end{pmatrix}$$

$$\times\begin{pmatrix}1 & 0\\ -\frac{1}{f_1} & 1\end{pmatrix}\begin{pmatrix}1 & \ell_1\\ 0 & 1\end{pmatrix}\begin{pmatrix}1 & 0\\ -\frac{1}{f_0} & 1\end{pmatrix} \tag{B1}$$

Using the confocal condition of $\ell_{BC}=f_1+f_2$ and the definition of the axicon magnification, $m=-f_1/f_2$, the round trip matrix can be reduced to

$$P=\begin{pmatrix}1-\frac{1}{f_0}2\ell_{eq} & 2\ell_{eq}\\ -\frac{1}{f_0} & 1\end{pmatrix} \tag{B2}$$

where $\ell_{eq}\equiv m\ell_{BC}+m^2(\ell_2+r_c)$.

The eigenvalues λ of Eq. (B2) are determined from

$$r=Pr_0=\lambda r_0 \tag{B3}$$

The eigenvalue solutions are then

$$\lambda=\lambda_a,\lambda_b=1-\frac{1}{f_0}\ell_{eq}\pm\sqrt{1-\frac{1}{f_0}\ell_{eq}^2-1} \tag{B4}$$

Since f_0 is negative and thus the λ_a solution is the larger, and let

$$\lambda_a=M \text{ and } \lambda_b=1/M \tag{B5}$$

where M is the geometric magnification of the resonator. Combining the above results we have

$$1/f_0\ell_{eq}=-(M-1)^2/2M \tag{B6}$$

Substituting Eq. (B6) into Eq. (B2), one obtains the round trip propagation matrix as

$$P=\begin{pmatrix}1+\frac{(M-1)^2}{M} & -\frac{(M-1)^2f_0}{M}\\ -\frac{1}{f_0} & 1\end{pmatrix} \tag{B7}$$

Using Eq. (B7) and $\lambda=M$, the edge ray height and slope are obtained as

$$r_0=\begin{pmatrix}a\\ -\frac{a}{f_0(M-1)}\end{pmatrix} \tag{B8}$$

where a is the radius of feedback mirror.

Similarly, the matrix for the propagation through the feedback mirror to the annular flat is obtained

$$P_a=\begin{pmatrix}\frac{M^2+1}{2mM} & -\frac{(M-1)^2f_0}{2mM}\\ -\frac{m}{f_0} & m\end{pmatrix} \tag{B9}$$

Then propagating the edge ray r_0 to the annular flat gives

$$r_4=P_ar_0=\begin{pmatrix}\frac{M+1}{2m}a\\ -\frac{mM}{(M-1)}\frac{a}{f_0}\end{pmatrix} \tag{B10}$$

Thus, the distance between edge ray and the annular optical axis W is

$$W=\frac{M+1}{2m}a \tag{B11}$$

This gives the required condition on the magnification of the axicon

$$m=\frac{a}{W}\frac{M+1}{2} \tag{B12}$$

The virtual source for the feedback ray being launched into the resonator is determined from

$$r=\begin{pmatrix}1 & 0\\ -\frac{1}{f_0} & 1\end{pmatrix}\begin{pmatrix}a\\ -\frac{a}{f_0(M-1)}\end{pmatrix}=\begin{pmatrix}a\\ \frac{Ma}{f_0(M-1)}\end{pmatrix} \tag{B13}$$

The virtual source radius is

$$z\approx -a\Big/\frac{Ma}{f_0(M-1)}=-\frac{M-1}{M}f_0=\left(\frac{M-1}{M}\right)\cdot\frac{2M}{(M-1)^2}\ell_{eq}$$

$$=\frac{2\ell_{eq}}{(M-1)} \tag{B14}$$

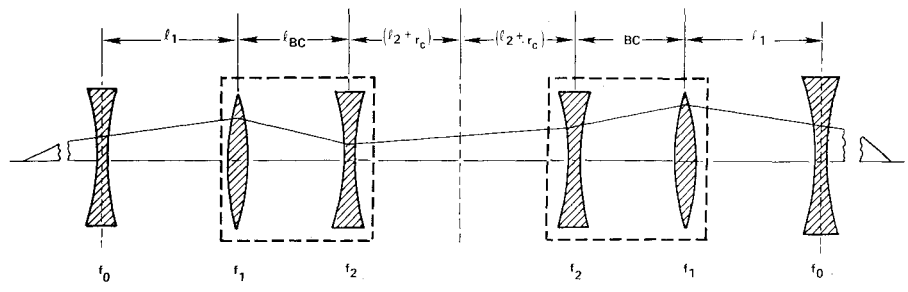

Fig. B1 Sequence of elements.

The virtual source distance $\bar{\ell}$ (see Fig. 1) for the parabolic-parabolic resonator in the annular region is determined from

$$\begin{pmatrix} \frac{1}{m} & \ell_{BC} \\ 0 & m \end{pmatrix} = \begin{pmatrix} 1 & \bar{\ell} \\ 0 & 1 \end{pmatrix} \begin{pmatrix} \frac{1}{m} & 0 \\ 0 & m \end{pmatrix} \tag{B15}$$

which results in

$$\bar{\ell} = \ell_{BC}/m \tag{B16}$$

The beam compactor of the $p-p$ resonator has the properties of mapping the coordinate and the radius of curvature in the compacted region r_1 and z_1 to the annular region in the following manner

$$\begin{pmatrix} \frac{1}{m} & 0 \\ 0 & m \end{pmatrix} \begin{pmatrix} r_1 \\ \frac{r_1}{z_1} \end{pmatrix} = \begin{pmatrix} r_2 - r_c \\ \frac{r_2 - r_c}{z_2} \end{pmatrix} \tag{B17}$$

or

$$r_1 = m(r_2 - r_c)$$

and

$$z_2 = z_1/m^2 \tag{B18}$$

The intensity distribution in the compacted region $I_1(r_1)$ is related to the intensity distribution in the annular region $I_2(r_2)$ as

$$I_1(r_1) = m(r_2/r_1) I_2(r_2) \tag{B19}$$

Acknowledgment

The author wishes to thank L. Moon, D. Holmes, J. Vieceli, L. Zajac and R. Swanson for valuable discussions. This work was supported in part by the Air Force Weapons Laboratory under Contract F29601-77-C-0006.

References

[1] Mirels, H., "Interaction between Unstable Optical Resonator and cw Chemical Lasers," *AIAA Journal*, Vol. 13, June 1975, pp. 785-791.

[2] Sentman, L. H., "Chemical Laser Power Spectral Performance: A Coupled Fluid Dynamics, Kinetic, and Physical Optics Model," *Applied Optics*, Vol. 17, July 1978, p. 2244.

[3] Mumola, P. B., Robertson, H. J., Steinberg, J. O., Kreuzer, J. L., and McCullogh, A. W., "Unstable Resonators for Annular Gain Volume Laser," *Applied Optics*, Vol. 17, March 1978, p. 936.

[4] Shapiro, A. H., *The Dynamics and Thermodynamics of Compressible Fluid Flow*, Ronald, New York, 1953, Chap. 8.

[5] Launder, B. E., "An Improved Pohlhausen-Type Method of Calculating the Two-Dimensional Laminar Boundary Layer in a Pressure Gradient," *Journal of Heat Transfer, ASME Transactions*, Aug. 1964, pp. 360-369.

[6] Wilkins, R. L., "Monte Carlo Calculations of Reaction Rates and Energy Distribution among Reaction Products II: $H + HF(v) \rightarrow H(v) \rightarrow H(v') + F$ and $H + HF(v) \rightarrow HF(v') + H$," *Journal of Chemical Physics*, Vol. 58, April 1973, pp. 3038-3046.

[7] Cohen, N. and Bott, J. F., "Kinetics of Hydrogen Halide Chemical Lasers," *Handbook of Chemical Lasers*, edited by R.W.F. Gross and J. F. Bott, John Wiley and Sons, New York, 1976, p. 32.

[8] Hall, R. J., "Rotational Nonequilibrium and Line Selected Operation in cw DF Chemical Lasers," *IEEE Journal of Quantum Electronics*, Vol. 12, Aug. 1976, p. 453.

[9] Chodzko, S. B., Mason, S. B., and Cross, E. F., "Annular Converging Wave Cavity," *Applied Optics*, Vol. 15, Sept. 1976, p. 2137.

[10] Casperson, L. W. and Shabbin Shekhani, M., "Mode Properties of Annular Gain Lasers," *Applied Optics*, Vol. 14, Nov. 1975, p. 2653.

[11] Freiberg, R. J., Fradin, D. W., and Chanausky, P. O., "Split-Mode Unstable Resonator," *Applied Optics*, Vol. 16, May 1977, pp. 1192.

[12] Rensch, D. B. and Chester, A. N., "Iterative Diffraction on Calculations of Transverse Mode Distribution in Confocal Unstable Laser Resonator," *Applied Optics*, Vol. 12, May 1973, p. 997.

[13] Statz, H. and O'Tang, C. L., "Problem of Mode Deformation in Optical Lasers," *Journal of Applied Physics*, Vol. 36, June 1965, pp. 1816-1818.

[14] Tregay, G. W., Janick, D. R., Wood, L. M., and Clune, E. F., "CL-XI Trip Nozzle Performance DF Small Signal Gain Measurements," Bell Aerospace Rept. 9276-928001, Jan. 1978.

[15] Wilson, L. and Hook, D., "Deuterium Fluoride CW Chemical Lasers," AIAA Paper 76-344, June 1976.

[16] Tregay, G. W. and Driscoll, R., "HF Chemical Laser Technology," Bell-Aerospace, Buffalo, New York, R&D Status Rept. 11, June 1978.

[17] *Handbook of Chemical Lasers*, edited by R. W. Gross and J. F. Bott, John Wiley & Sons, New York, 1976, Sec. 3.2.

[18] Gerrard, A. and Burch, J. M., *Introduction to Matrix Methods in Optics*, John Wiley & Sons, New York, 1975.